AD-A033 075 MARTIN MARIETTA LABS BALTIMORE MD F/G 12/1
INTEGRATING OF THE 3-D HARMONIC KERNEL.(U)
AUG 76 P F JORDAN F44620-73-C-0041
UNCLASSIFIED MML-TR-76-46C AFOSR-TR-76-0948 NL

| OF |
AD
A033075

END

DATE
FILMED
2-77

MARTIN MARIETTA

Martin Marietta Laboratories

(12)

MML TR 76-46c

INTEGRATION OF THE 3-D HARMONIC KERNEL

Peter F. Jordan

August 1976

AFOSR Scientific Report

Prepared for:
Air Force Office of Scientific Research (AFSC)
Bolling Air Force Base, D.C. 20332
Under Contract F44620-73-C-0041

MML TR 76-46c

INTEGRATION OF THE 3-D HARMONIC KERNEL

by

Peter F. Jordan

MARTIN MARIETTA CORPORATION
Martin Marietta Laboratories
1450 South Rolling Road
Baltimore, Maryland 21227

August 1976

Prepared for
DEPARTMENT OF THE AIR FORCE
Air Force Office of Scientific Research (AFSC)
Bolling Air Force Base, Washington, D. C. 20332

Under Contract F44620-73-C-0041

UNCLASSIFIED

SECURITY CLASSIFICATION OF THIS PAGE (When Data Entered)

REPORT DOCUMENTATION PAGE

READ INSTRUCTIONS BEFORE COMPLETING FORM

1. REPORT NUMBER: AFOSR-TR-76-0948
2. GOVT ACCESSION NO.
3. RECIPIENT'S CATALOG NUMBER

4. TITLE (and Subtitle): INTEGRATION OF THE 3-D HARMONIC KERNEL.
5. TYPE OF REPORT & PERIOD COVERED: INTERIM rept.,
6. PERFORMING ORG. REPORT NUMBER: MML-TR-76-46c

7. AUTHOR(s): PETER F. JORDAN
8. CONTRACT OR GRANT NUMBER(s): F44620-73-C-0041

9. PERFORMING ORGANIZATION NAME AND ADDRESS:
MARTIN MARIETTA CORPORATION
MARTIN MARIETTA LABORATORIES
1450 SOUTH ROLLING ROAD
BALTIMORE, MARYLAND 21227

10. PROGRAM ELEMENT, PROJECT, TASK AREA & WORK UNIT NUMBERS: 681307 / 9781-02 / 61102F
17. 02

11. CONTROLLING OFFICE NAME AND ADDRESS:
AIR FORCE OFFICE OF SCIENTIFIC RESEARCH/NA
BLDG 410
BOLLING AIR FORCE BASE, D C 20332

12. REPORT DATE: AUGUST 1976
13. NUMBER OF PAGES: 25

14. MONITORING AGENCY NAME & ADDRESS (if different from Controlling Office): 27p.

15. SECURITY CLASS. (of this report): UNCLASSIFIED
15a. DECLASSIFICATION/DOWNGRADING SCHEDULE

16. DISTRIBUTION STATEMENT (of this Report)

Approved for public release; distribution unlimited.

17. DISTRIBUTION STATEMENT (of the abstract entered in Block 20, if different from Report)

18. SUPPLEMENTARY NOTES

19. KEY WORDS (Continue on reverse side if necessary and identify by block number)
UNSTEADY AERODYNAMICS
UNSTEADY LIFTING SURFACE THEORY
FINITE ELEMENTS
SINGULAR INTEGRALS

20. ABSTRACT (Continue on reverse side if necessary and identify by block number)

Currently, the singular integral that arises in the analysis of oscillating lifting surfaces is evaluated by approximate methods, and considerable scatter exists between the results of different methods. In this paper, the application of an accurate approach to the Falkner finite element method is described, and some numerical results are compared with two current levels of approximation.

DD FORM 1 JAN 73 1473 EDITION OF 1 NOV 65 IS OBSOLETE

UNCLASSIFIED

407 998

CONTENTS

One Table; five figures.

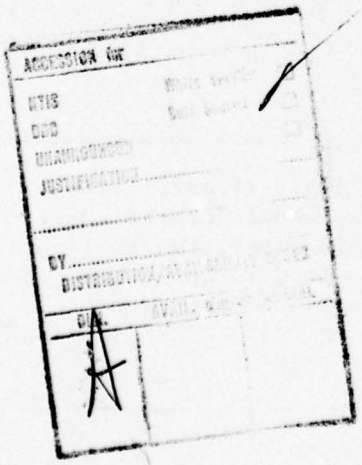

INTRODUCTION

This note is concerned with a problem of numerical evaluation that arises in the analysis of oscillating lifting surfaces; its purpose is to indicate a method of obtaining accurate solutions where no such method seemed to exist, and to illustrate the magnitude and the nature of the errors that arise from current approximate methods. Completeness is not intended; that is, while given problems may involve various complications, depending on the model at hand, those complications that are not relevant for the intended demonstration of a basically different approach will not here be considered. Rather, we assume the simplest model, the planar wing in incompressible flow. (The planform of the wing is not of concern.)

Also, while the new approach may be generalized, we confine our discussion to a specific finite element method of solution, namely, to the Falkner method. In finite element methods, generally, the surface is treated as a composite of finite elements E_n; one requires the aerodynamic influence coefficients $w_{s,n}$, which measure the downwash due to unit (oscillating) lift on any "sending" element E_s, on pre-determined collocation points (x_n, y_n) on the "receiving" elements E_n (which include E_s).

In the Falkner "horseshoe vortex" method (also called "doublet-lattice" method, see, e.g., Ref. 1) the sending element E_s is modeled by a horseshoe vortex the bound part of which (i.e., the part that produces the lift) spans the 1/4-chord line of E_s. For this model, we will first give an indirect (and tentative) indication of the likely distribution of

the errors which arise from a specific approximative method, here to be called the "parabolic approximation"[1]. We will then show how the $w_{s,n}$ can be calculated to arbitrary accuracy, and will demonstrate numerically, for the two most critical $w_{s,n}$, the errors that exist at two different levels of approximation. Finally, we will briefly discuss the status of the overall problem and its remaining difficulties.

FORMULATION

We will use exclusively the configuration of elements E_n which is shown in Fig. 1. The E_n are equal squares. The x-axis is parallel to the undisturbed flow speed, V, and is centered on the sending element E_s. The bound vortex lies on the y-axis. Both coordinates, x and y, are referred to the length ℓ; 2ℓ is the side length of each E_n. The same length ℓ we use to define the reduced frequency

$$k = \omega \ell / V \tag{1}$$

By unit lift (above) we imply that the lift coefficient of E_s is

$$C_{L,s} = 1 \cdot \exp(i\omega t) \tag{2}$$

The influence coefficient $w_{s,n}$ measures the dimensional downwash W_s at the collocation point (x_n, y_n) as follows:

$$\pi W_s(x_n, y_n) = w_{s,n} V \cdot \exp(i\omega t) \tag{3}$$

Though we will require only individual influence coefficients $w_{s,n}$, these are really individual values of a continuous (in general) function $w_s(x, y; k)$, and in our analysis it is more convenient to

use this functional form. With the definitions introduced above, this influence function is given by an integral of the form

$$w_s(x, y;k) = -\frac{1}{4\pi} \int_{-1}^{+1} K(x, |y-\eta|, k) \frac{d\eta}{(y-\eta)^2} \qquad (4)$$

All the terms in Eq. (4) are non-dimensional. The detailed form of the kernel K we will discuss later.

Whenever y=0 (i.e., when E_n is centered on the x-axis) the integral in Eq. (4) is a Hadamard integral, singular to second order. On the other hand, the kernel K is given numerically and to limited accuracy. For this reason, presumably, the scatter between results obtained by various current methods is around 10%.[2] This is not satisfactory; our goal is to obtain accurate, reliable results.

THE PARABOLIC APPROXIMATION

In this section we want to illustrate, though in an indirect manner (by means of readily available exact results) the working of a current approximate method. Our purpose is to obtain a tentative indication as to which parameter range should be of foremost concern.

In the steady limit (k=0), Eq. (4) can readily be resolved analytically, since here the kernel takes the simple form

$$K^{(s)} = 1 + x/(x^2 + (y-\eta)^2)^{\frac{1}{2}} \qquad (5)$$

The suffix (s) in $K^{(s)}$ denotes "steady".

In the method proposed in Ref. 1, the unsteady part $K^{(u)}$ is defined by

$$K = K^{(s)} + K^{(u)} \tag{6}$$

This rather complicated part is approximated by the parabola through its values for $\eta = -1$, $\eta = 0$ and $\eta = 1$. The integration over this parabola is performed analytically, and the "parabolic approximation" to the unsteady part $w_s^{(u)}(x, y)$ of the influence function is thus obtained. By adding the known exact contribution of $K^{(s)}$, one obtains an approximate value for the complete influence function $w_s(x, y; k)$.

We apply here the parabolic approximation to $K^{(s)}$ (rather than to $K^{(u)}$) and can then compare this approximation with the known exact result. For example, for y=0 the approximation is

$$2w_s^{(s)}(x, 0; 0) = \begin{Bmatrix} 3 \\ -1 \end{Bmatrix} - x/(1+x^2)^{\frac{1}{2}} \qquad (x \gtrless 0) \tag{7}$$

and the exact result is

$$2\, w_s^{(s)}(x, 0; 0) = 1 + (1+x^2)^{\frac{1}{2}}/x \tag{7a}$$

Numerical values are listed in Fig. 1 (where, as is characteristic for the Falkner method, the central 3/4-chord point of each E_n is used as its collocation point). The correct result, Eq. (7a), is written above each collocation point, the error Δw_s in the approximation Eq. 7 is written underneath. A bar (-) underneath indicates that the (absolute) error is <0.0001.

The errors listed in Fig. 1 (antisymmetric with respect to the y-axis) converge to zero rapidly away from E_s -- much more rapidly than the w_s themselves converge toward their respective limits. Sizable errors arise on and near E_s; the largest errors arise along the x-axis (where the integral in Eq. (4) is singular). Along this axis, exact influence function and approximation are shown in Fig. 2, where it is seen that the error becomes infinite as the bound vortex is approached. In Fig. 1, the largest percentage error is 29% (at the collocation point (-1, 0)) and is thus rather large.

Away from the x-axis, the errors listed in Fig. 1 are much smaller, an important reason being that outside the bound vortex the error at x=0 is zero rather than infinite. The largest errors along the verticals $y = \pm 2$ are $\Delta w_s = \pm 0.0009$ at $x = \pm 0.5$.

AN ACCURATE METHOD

a. General

In the case of unsteady flow, the kernel K is given by the integral

$$K = \int_{-x/|y-\eta|}^{\infty} \exp(-ik(x+|y-\eta|\,u)) \frac{du}{(1+u^2)^{3/2}} \qquad (8)$$

To evaluate Eq. (8) directly means that one has to deal with incomplete cylinder functions. The evaluation method proposed in Appendix A of Ref. 1 is not particularly accurate.* There are thus two distinct sources of possible error: the evaluation of K, and the parabolic approxi-

*A new, slightly simpler but much more accurate method is presented in Ref. 3.

mation. One would tend to expect that the second source would produce the larger errors and, therefore, would tend to expect that the largest errors will again arise at the collocation points ($\pm$ 1, 0) as in Fig. 1. On this basis and in order to simplify the presentation of the essence of our method, we assume in the present section that y = 0. For brevity, then, we write $w_s(x;k)$ for $w_s(x, 0;k)$. (In fact, as we will see later (Eq. 18), $w_s(x, y;k)$ can always be expressed by $w_s(x;k)$.)

Equation (4) with Eq. (8) inserted presents a double integral. The essence of our approach is that, by reversing the sequence of integration, we avoid the incomplete cylinder functions. (That this reversal is permitted one checks most readily in the steady case. Here all integrations can be performed analytically in either sequence, and the same result is obtained either way.)

Setting y=0, $u\eta=\zeta$, and reversing, one obtains

$$-2w_s(x;k)e^{ikx} = \int_{-x}^{\infty} e^{-ik\zeta}\left(\int_0^1 \frac{d\eta}{(\eta^2+\zeta^2)^{3/2}}\right)d\zeta = \int_{-x}^{\infty} \frac{e^{-ik\zeta}d\zeta}{\zeta^2(1+\zeta^2)^{\frac{1}{2}}} \equiv J(-x) \quad (9)$$

The problem of determining w_s has been reduced to that of evaluating the single (complex) integral J(-x). The real and imaginary parts of this integral we will denote as follows

$$J(x) = J^c(x) - iJ^s(x) \quad (9a)$$

the suffix c indicating cos, the suffix s indicating sin in the integrand.

The integral J is not difficult to evaluate, but different methods are required in different ranges of the variable ζ. To indicate an integral that extends from ζ = a to ζ = b, we write J(a, b), but we usually omit the

upper limit if this limit is ∞. Thus

$$J(a) \equiv J(a,\infty) = J(a,b) + J(b) \tag{9b}$$

The singularity at $\zeta = 0$ enters if x is positive but not if x is negative, and this turns out to be a major distinction. In order to avoid confusion of signs (and a clumsy notation), we introduce p to mean $|x|$. We deal first with the case $x \leq -1$ where there is no singularity.

b. The Case $x \leq -1$

Writing v for $k\zeta$, we have

$$J^c(p) = k^2 \int_{kp}^{\infty} \frac{\cos v}{(1+(k/v)^2)^{\frac{1}{2}}} \frac{dv}{v^3} = \sum_{\nu=1}^{\infty} J_\nu^c(p) \tag{10}$$

with $$J_\nu^c(p) = (-)^{\nu-1} \bar{\nu}\, k^{2\nu} \int_{kp}^{\infty} \frac{\cos v\, dv}{v^{2\nu+1}} \tag{10a}$$

where $$\bar{\nu} \equiv \frac{1\cdot 3\cdot 5\cdots(2\nu-1)}{2\cdot 4\cdot 6\cdots(2\nu)} \; ; \quad \bar{0} = 1 \tag{10b}$$

The same formulas apply to $J^s(p)$ if cos is replaced by sin. The two types of elementary integrals are given in Ref. 4, formulas 333:7b and 6b. After rearrangement, they take the forms

$$\tfrac{1}{2}J^c(p) = A\cos(kp) - kB\sin(kp) + k^2 C\,Ci(kp) \tag{11a}$$

$$\tfrac{1}{2}J^s(p) = A\sin(kp) + kB\cos(kp) + k^2 C\,si(kp) \tag{11b}$$

The functions Ci and $si \equiv Si - \pi/2$ are the cosine and sine integrals (e.g., Ref. 5, formulas 5.2.1, 2&5). These may be calculated to very high accuracy by means of IBM Subroutine SICI, Ref. 6, p. 370.

Insertion of Eqs. (11a, b) into Eq. (9) yields

$$w_s(x;k) = -A + ikB - k^2[\,Ci(kp) - isi(kp)\,]Ce^{ikp} \quad (x \le -1) \tag{12}$$

If the argument kp is large, Ci and si are best expressed by the functions $f(z) \sim 1/z$, $g(z) \sim 1/z^2$, see formulas 5.2.8, 9, 34 & 35 of Ref. 5. Then

$$w_s(x;k) = -A + ikB - k^2[\,if(kp) - g(kp)\,]C \tag{12a}$$

No oscillatory term is left in this asymptotic form.

The functions A, B and C of Eq. (11) are given by series:

$$A = \sum_0^\infty k^{2n} A_n = \frac{1}{2p^2} \sum_0^\infty k^{2n} \sum_{\nu=0}^\infty (-)^\nu \frac{A_{n,\nu}}{p^{2\nu}} \tag{13a}$$

$$B = \sum_0^\infty k^{2n} B_n = \frac{1}{2p} \sum_0^\infty k^{2n} \sum_{\nu=0}^\infty (-)^\nu \frac{B_{n,\nu}}{p^{2\nu}} \tag{13b}$$

$$C = \sum_0^\infty k^{2n} C_n = \frac{1}{2} \sum_0^\infty k^{2n} \cdot \frac{\bar{n}}{(2n+2)!} \tag{13c}$$

$$A_{n,\nu} = (2\nu+1)B_{n,\nu} \; ; \quad B_{n,\nu} = \frac{\overline{n+\nu}\;(2\nu)!}{(2n+2\nu+2)!} \tag{13d, e}$$

Note that

$$2A_0 = -1 + (1+p^2)^{\frac{1}{2}}/p \tag{13f}$$

If one sets k=0 in Eq. (12), all terms on the right disappear except $-A_0$, and the steady flow result Eq. (7a) is thus recovered.

Noting further that

$$A_{n,0} = B_{n,0} = C_n \tag{13g}$$

one sees that one can simplify by splitting off the terms $\nu = 0$, setting

$$A = C/p^2 - \bar{A}; \quad B = C/p - \bar{B} \qquad (13h, k)$$

so that Eq, (12) becomes, again for $x \leq -1$,

$$w_s(x;k) = -\{1/p^2 - ik/p + k^2[Ci(kp) - isi(kp)]e^{ikp}\} C + \bar{A} - ik\bar{B} \qquad (14)$$

The factor C is quickly calculated:

$$C = \frac{1}{4} + \frac{k^2}{96} + \frac{k^4}{3840} + \frac{k^6}{258048} + \ldots \qquad (14a)$$

The remainder terms we write as

$$\bar{A} = \sum_0^\infty k^{2n} \bar{A}_n(p) \; ; \quad \bar{B} = \sum_0^\infty k^{2n} \bar{B}_n(p) \qquad (14b, c)$$

Sample numerical values are given in Table 1; using these, one can quickly find $\bar{A}$ and $\bar{B}$ if $p = 1$, 2 or ≥ 3. For p-values in between*, only $\bar{A}_o$ and $\bar{B}_o$ may be required if k is small enough and/or if p is large enough. Of these, $\bar{A}_o$ can be calculated from its analytical form, compare Eq. (13f)

$$\bar{A}_0 = [1 + 1/2p^2 - (1+1/p^2)^{\frac{1}{2}}]/2 \qquad (14d)$$

On the other hand, the series $\bar{B}_o$ converges rather slowly if p is close to 1. Fortunately, one has an easy and quick alternative in all the cases when evaluation of the double series becomes inconvenient; returning to Eq. (9), one calculates the part-integral J(p, b) (with either b=2 or b=3) by numerical integration, and determines the remaining integral J(b) using Table 1.

---

*In Fig. 1, x is always an odd interger. Other values of x do arise, however, e.g. in compressible flow, or when $\gamma \neq 0$, see Eq. (18) below.

c. The Case $x > +1$

If $x \geq +1$, then $x = p$, and from the symmetry properties of the circular functions follows that

$$J^c(-p) = 2J^c(0) - J^c(p) \; ; \; J^s(-p) = J^s(p) \qquad (15a, b)$$

Therefore, Eq. (9) takes the form

$$w_s(x;k)e^{ikx} = \tfrac{1}{2}J^c(x) - J^c(0) + \frac{i}{2}J^s(x) \quad (x \geq +1) \qquad (16)$$

An alternate form of Eq. (16) is sometimes useful:

$$w_s(x;k) = -\mathrm{Re}w_s(-x;k) + i\mathrm{Im}w_s(-x;k) - J^c(0)e^{-ixk} \qquad (16a)$$

Of the terms on the right of Eq. (16), only the part-integral $J^c(0, 1)$ has not already been disucssed in the preceding. For this integral we have

$$-J^c(0, 1) = -\int_0^1 \frac{\cos k\zeta \, d\zeta}{\zeta^2(1+\zeta^2)^{\frac{1}{2}}} = \sum_0^\infty k^{2\nu} I_\nu \qquad (17)$$

The elementary integrals

$$I_\nu = \frac{(-)^{\nu+1}}{(2\nu)!}\int_0^1 \frac{\zeta^{2\nu-2} d\zeta}{(1+\zeta^2)^{\frac{1}{2}}} \qquad (17a)$$

are standard integrals (e.g., Ref. 4, section 234). Their numerical values converge to zero rapidly as ν increases; see Table 2.

When x is large (and positive), the integral $J^c(0)$ provides by far the largest contribution to $w_s(x;k)$, and this contribution is oscillatory. Herein lies a pronounced distinction between the ranges of large positive x and of large negative x, Eq. (12a).

(d) The Case $x < 1$

In this case one requires the part-integrals $J^c(p, 1)$ and $J^s(p, 1)$. Series presentations corresponding to Eqs. (17), (17a) can be used but will be less convenient then direct numerical integration (except if k is quite small). Equations (16) and (16a) remain applicable.

NUMERICAL EXAMPLES

The largest errors from applying the parabolic approximation to the steady flow problem occurred (see Fig. 1) at the collocation points closest to the bound vortex, that is, at the points $(x, y) = (\pm 1, 0)$. For these points we have calculated (for the range $0 \leq k \leq 1$) the following sets of results:

(a) the accurate influence coefficients w_s;

(b) the w_s calculated by applying the parabolic approximation to only the unsteady part $K^{(u)}$ of the kernel, using accurate values for $K^{(u)}$;

(c) the corresponding parabolic approximations calculated using the less accurate values for $K^{(u)}$ that one obtains using the method proposed in Appendix A of Ref. 1.

In Figs. 3 to 5 some of these results are presented and are denoted by "correct", "parabolic approximation", and "Ref. 1", respectively.

Figure 3 refers to the frontal point (-1, 0) and shows results (a) and (b). The real parts are denoted by Re, the imaginary parts by Im. The phase angle is $\pi/2 - \phi$. While there is sufficient similarity between

the two sets of results (calculated by quite different methods) to create confidence in the correctness of the evaluation, there are also considerable errors in (b), in particular when k is large. The same comment applies to Fig. 4 where the corresponding results are shown for the collocation point on E_s. (The two curves for ϕ almost coincide in the case of Fig. 4 and are not shown).

(Note that the antisymmetry of the errors in Fig. 1 is not repeated by the unsteady parts of the errors: those in Fig. 4 are much the larger.)

Superficially, one might be tempted to conclude from Figs. 3 and 4 that, by making k small enough (i.e., by using enough elements E_n) one could make all errors due to the parabolic approximation small enough to make them negligible. However, this would be a rather doubtful conclusion. Imagine a wing having a fixed reference reduced frequency $k_{c/2}$. As one decreases k, one decreases all the unsteady parts $w_s^{(u)}$ of the influence coefficients themselves; nevertheless, the solution (the unsteady pressure distribution) must be almost independent of k and must converge to the correct solution as $k \to 0$. In other words, as the $w_s^{(u)}$ decrease, their number increases. The process $k \to 0$ is not simple and requires some detailed study, but it seems clear enough that percentage errors should be more directly instructive than the absolute errors that are shown in Figs. 3 and 4.

Percentage errors in the unsteady parts $w_s^{(u)}$ are shown in Fig. 5.* For $Re^{(u)}$ (x = +1) no percentage curve is drawn because here there is a sign reversal in the correct curve, Fig. 4; in this case, the

---

*They are usually entered as positive, regardless of their actual sign (which can be read from Figs. 3 and 4).

error due to the parabolic approximation is 48% when k=0.1, 62% when k=0.2. The percentages that constitute the error curves in Fig. 5 are smaller than these values but are still fairly large even when $k \to 0$.

Also shown in Fig. 5 are some "Ref. 1" results. The additional error that arises from the inaccuracy in the K-values is relatively small, particularly when k is large, but occasionally it can be quite large, see the point for k=0.1 of $Re^{(u)}(x = -1)$. This particular point is a consequence of the "corner error" which is discussed in Ref. 3. This large error is disturbing because k=0.1 is well within the range of normal usage.

As an additional numerical example we compared for k=0.2 the unsteady contributions to the sets (a) and (b) at larger (positive and negative) values of x (up to p = 12). We found that the errors (in (b)) were not large (they are rather small, for k=0.2, even when p=1, see Figs. 3 and 4) but they did not exhibit either the rapid convergence to zero that is shown for the steady case in Figs. 1 and 2. Rather, in the unsteady example the percentage errors tended to stay about constant. Thus, while in the steady case the parabolic approximation was seen to be quite adequate for all collocation points sufficiently removed from the bound vortex, this desirable property is less pronounced, at best, in the unsteady case.

THE CASE $y \neq 0$

If $y \neq 0$, η^2 in the denominator of the inner integral in Eq. (9) has to be replaced by $(\eta - y)^2$, and

$$\frac{1}{2}\int_{-1}^{+1} \ldots d\eta \quad \text{replaces} \quad \int_{0}^{1} \ldots d\eta$$

It is then easily shown that (read y as $|y|$)

$$w_s(x, y;k) = \frac{1}{2}\left[\frac{1}{y+1} w_s\left(\frac{x}{y+1};k(y+1)\right) - \frac{1}{y-1} w_s\left(\frac{x}{y-1};k(y-1)\right)\right] \qquad (18)$$

The case $y \neq 0$ is thus formally reduced to the already resolved case $y=0$.

The fact that two coefficients (on the right) are required to form one (on the left) is not a duplication of effort, since those on the right will each be required with two different values of y. Of more concern is the fact that the effective reduced frequencies on the right, e.g. $k(y+1)$, may become larger (except if the wing aspect ratio is small) than the limit $k \leq 1$ for which our Tables 1 and 2 have been prepared. However, these sequences of coefficients exhibit rapidly increasing convergence as they are lengthened; we found that going to $k=3$ required only about two more terms. Furthermore, the high accuracy provided may be more than is required.

In many cases, the present tables will be sufficient. Extension of the tables, if required, is trivial. At worst, one can make more extensive use of direct numerical integrations.

REMARK ON EXTRAPOLATION

The overall goal of the present investigation (an earlier result of which was Ref. 3) is to calculate reliable reference solutions for certain problems in harmonic lifting surface theory. We aim to use finite elements and to perform extrapolations $k \to 0$; this approach was provoked by unexpectedly favorable results in steady flow analyses. As an example, consider a square wing, divided into N^2 equal square elements E_n. Use

two different types of sending elements E_s, the Falkner horseshoe vortex ("F") and the Woodward[7] element ("W") (here the lift is evenly distributed over E_s; however, we used collocation points at 85% chord while Woodward had proposed 95%). With each E_s, solve the (steady) problem of the flat square wing at incidence for three values N and extrapolate as follows:

$$C_{L\alpha, N \to \infty} \equiv C_{L\alpha} = C_{L\alpha, N} + (a/N) + (b/N^2)$$

In each case, the three results determine the three unknown constants $C_{L\alpha}$, a and b. We found

$C_{L\alpha} = 1.4597$ ("F") and 1.4602 ("W") with N = 4, 6 and 8

and found

$C_{L\alpha} = 1.4600$ ("F") and 1.4601 ("W") with N = 6, 8 and 10.

This is a remarkable success. In particular concerning the element "F", numerous investigations have been made relating to 2-D flow (where exact solutions are available for comparisons). Here we see a result for a small aspect ratio wing, a result obtained with little numerical effort, which shows that the two rather different types of elements E_s lead to the same result (the present result agrees with, but is more accurate than, any of the lift slope values for the square wing found in the literature). This observation serves to establish the validity of the finite element approach in lifting surface analyses.

The present investigation indicates that the same extrapolative approach may involve complications in the case of unsteady flow. Since one will keep the reference frequency $k_{c/2}$ constant, the element frequency

k will decrease like $1/N$ as N is increased, and the unsteady parts $w_s^{(u)}$ of the coefficients w_s will decrease correspondingly while the steady parts $w_s^{(s)}$ remain constant. This occurs in face of the goal to determine the specific effects of the $w_s^{(u)}$. Furthermore, the log k term in Ci(k) will affect the limit behavior as $N \to \infty$.

It thus appears that the goal of calculating reliable solutions to problems in unsteady lifting surface theory requires further analytical considerations and numerical experimentation.

CONCLUSION

To solve problems of harmonic lifting surface theory by means of finite element methods requires the determination of influence coefficients and, in particular, requires evaluation of singular integrals. An accurate method of performing this task has been demonstrated. Current methods (like the "parabolic approximation" to the kernel K of the integral) may lead to sizable errors. Further errors which arise from inaccurately evaluating K are usually relatively small but may become excessive when the reduced frequency k is small.

REFERENCES

1. Giesing, J. P., Kalman, T. P., and Rodden, W. P., "Subsonic Unsteady Aerodynamics for General Configurations." AFFDL-TR-71-5, Part I, Vol. I (November 1971).

2. Rodden, W. P., letter to the author dated 17 June 1975.

3. Jordan, P. F., "Numerical Evaluation of the 3-D Harmonic Kernel." MML TR 76-34c; AFOSR-TR-76-0004 (August 1975). Zeitschrift für Flugwissenschaften 24 (1976) p. 205.

4. Gröbner, W., and Hofreiter, N., "Integraltafel", Part I. Springer 1965.

5. Abramowith, M., and Stegun, I. A., eds., "Handbook of Mathematical Functions." Nat. Bureau of Standards, 3rd printing (1965).

6. IBM System/360 Scientific Subroutine Package (August 1970).

7. Woodward, F. A., "Analysis and Design of Wing-Body Combinations at Subsonic and Supersonic Speeds", J. Aircraft 5 (1968) p. 528.

Table 1. Coefficients in Remainder Terms, Eqs. (14b, c)

	p = 1	p = 2	p = 3	p > 3
$\bar{A}_0$	0.042893	0.003483	0.000732	$1/16p^4 - 1/32p^6 + 5/256p^8$
$\bar{A}_1$	0.001227	0.000092	0.000019	$1/640p^4$
$\bar{A}_2$	0.000020	0.000001	0	0
$\bar{B}_0$	0.016420	0.002428	0.000747	$1/48p^3 - 1/160p^5$
$\bar{B}_1$	0.000448	0.000062	0.000019	$1/1920p^3$
$\bar{B}_2$	0.000007	0.000001	0	0

Table 2. Elementary Integrals I_ν, Eq. (17a)

$I_0 = \sqrt{2} = +1.414214$

$I_1 = \frac{1}{2}\log(1+\sqrt{2}) = +0.440687$

$I_2 = (2I_1 - \sqrt{2})/48 = -0.011101$

$I_3 = (6I_1 - \sqrt{2})/5760 = +0.000214$

$I_4 = (30I_1 - 13\sqrt{2})/1935360 = -0.000003$

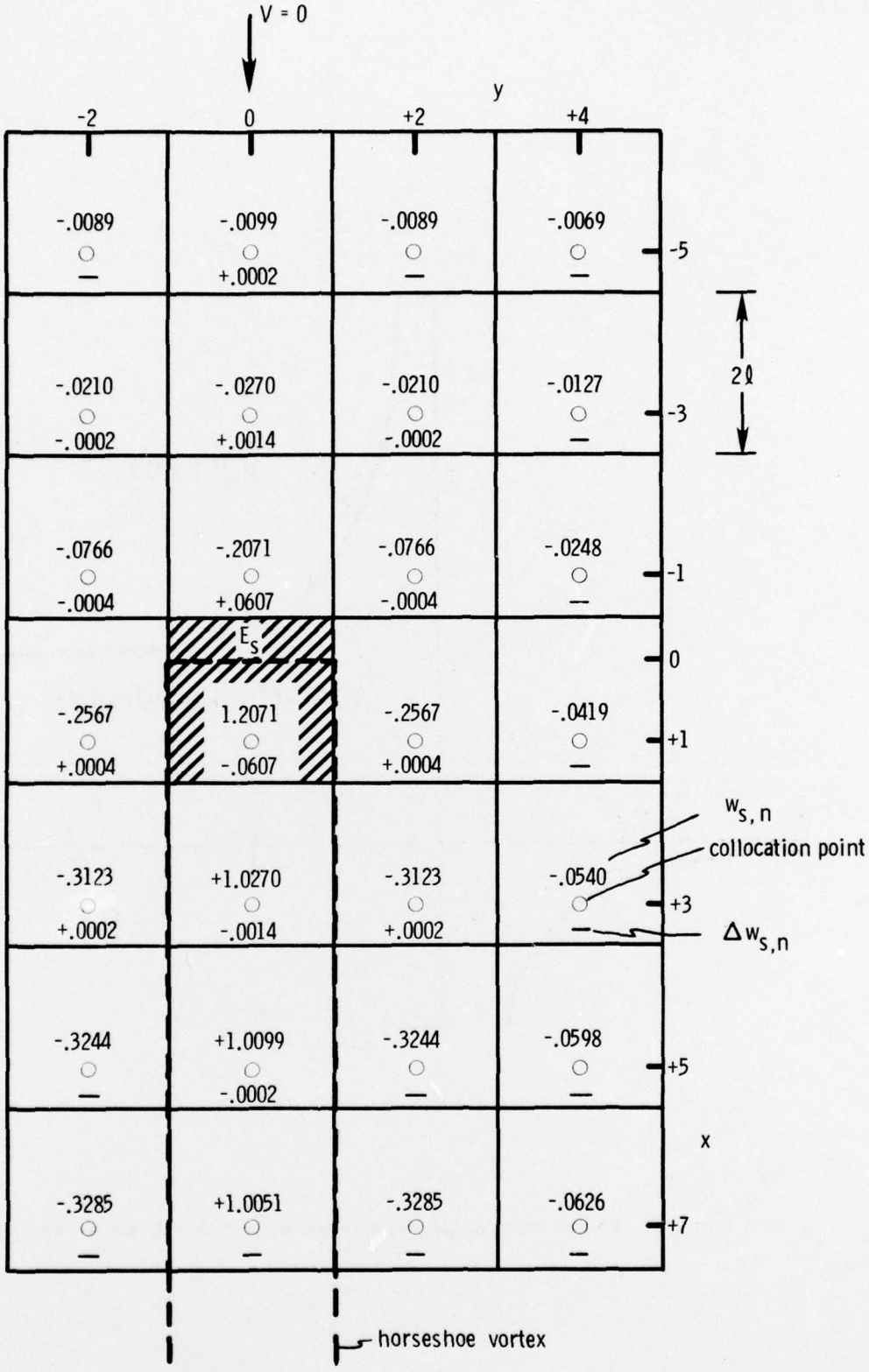

Fig. 1: Coordinates, elements E_n and influence coefficients (k=0).

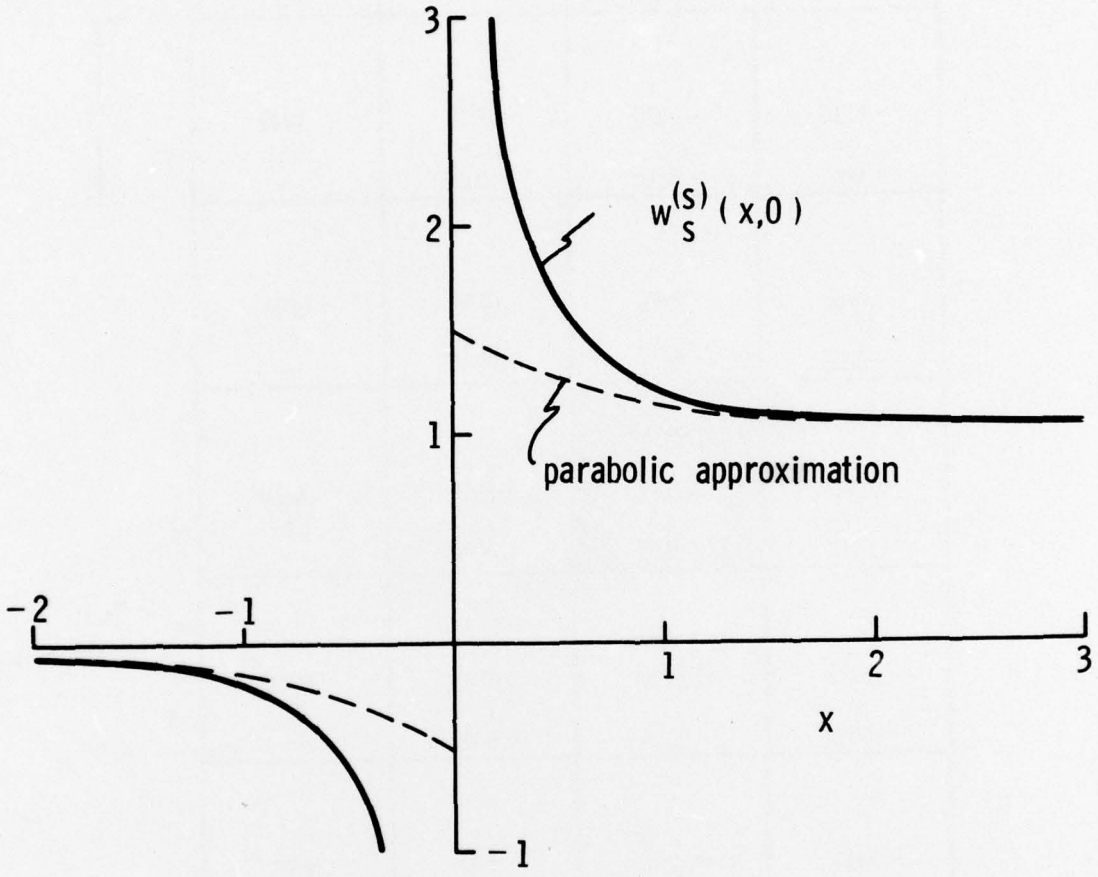

Fig. 2: Parabolic Approximation along the x-axis (k=0).

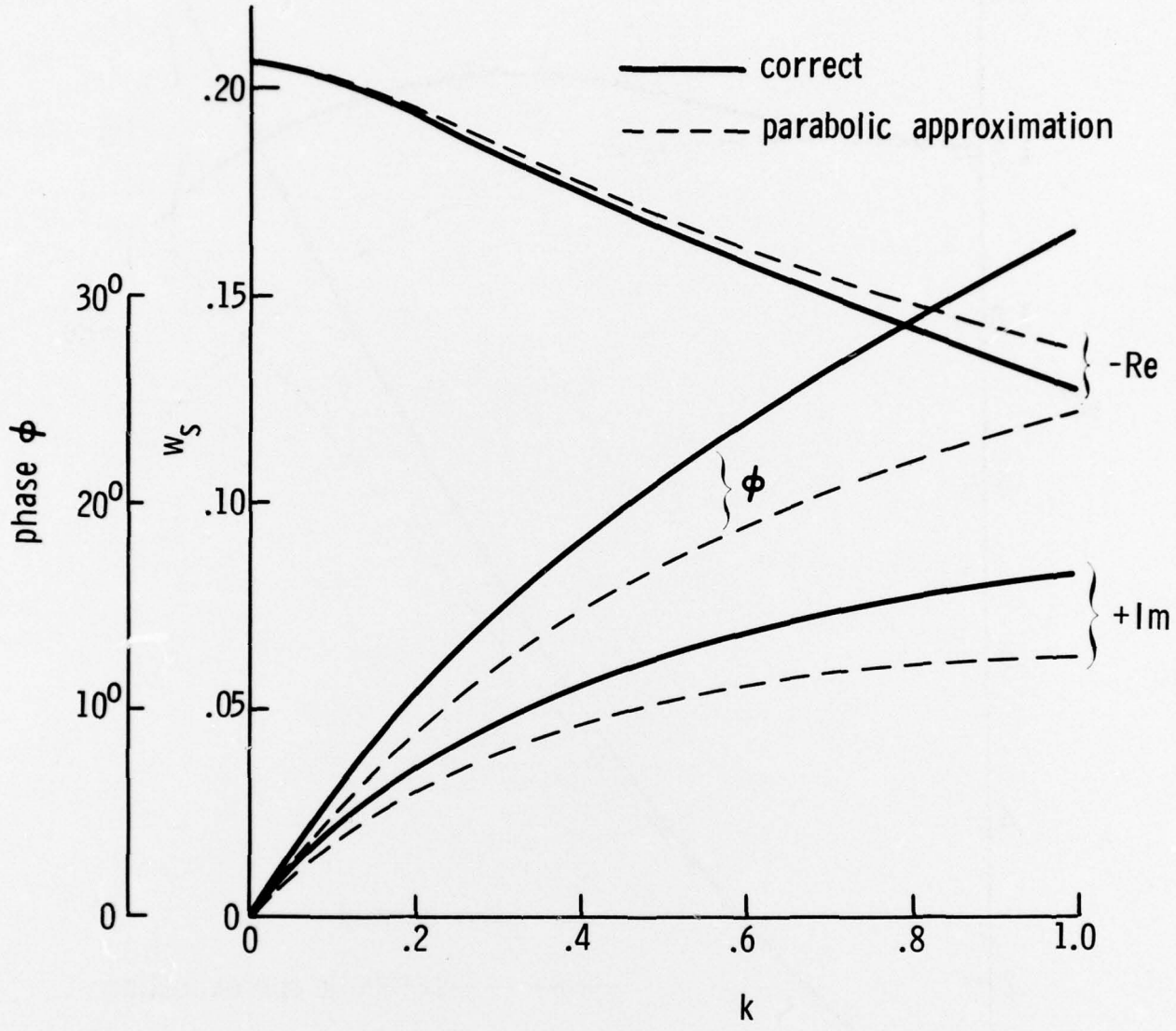

Fig. 3: Influence coefficient $w_s(-1;k)$.

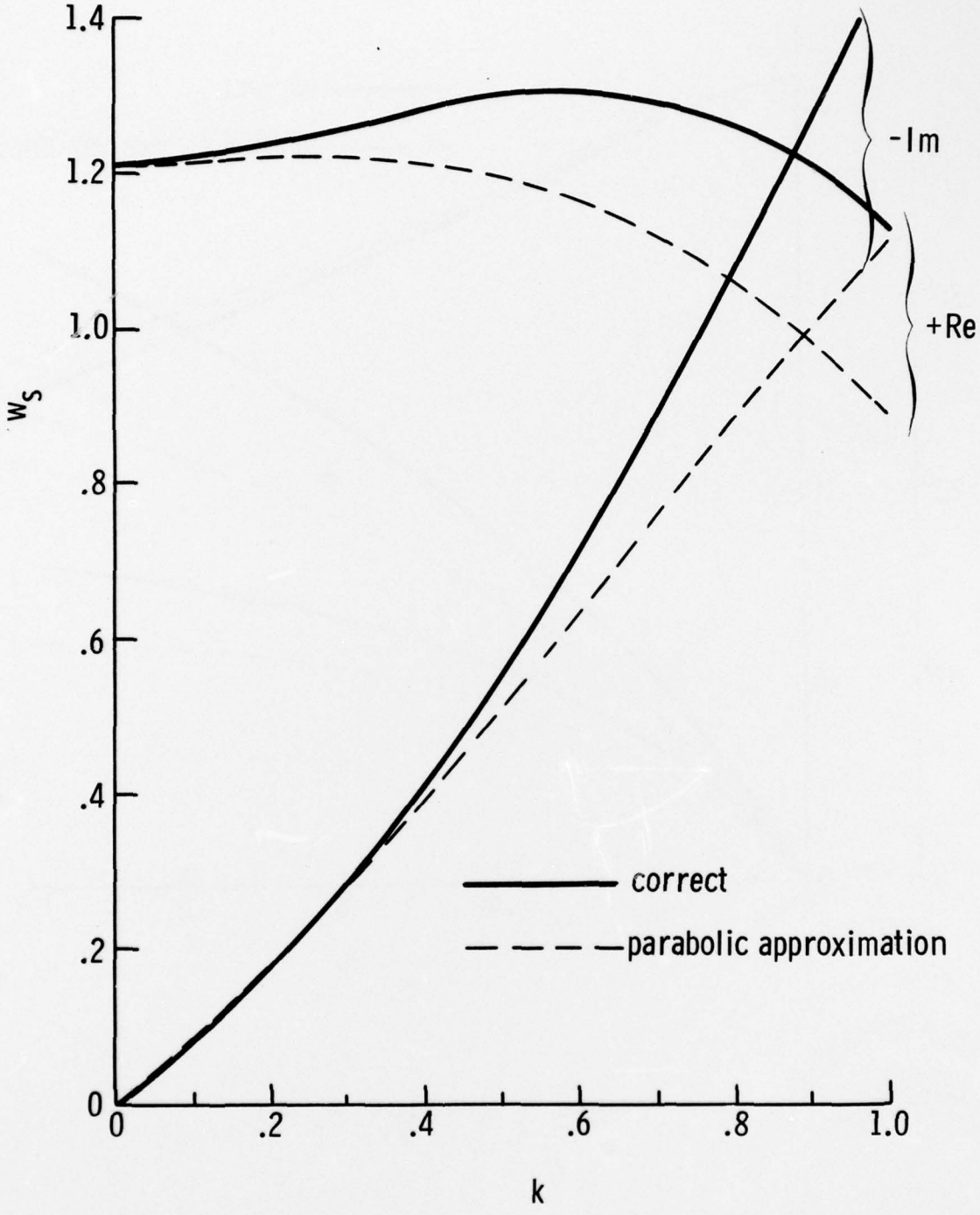

Fig. 4: Influence coefficient $w_s(+1;k)$.

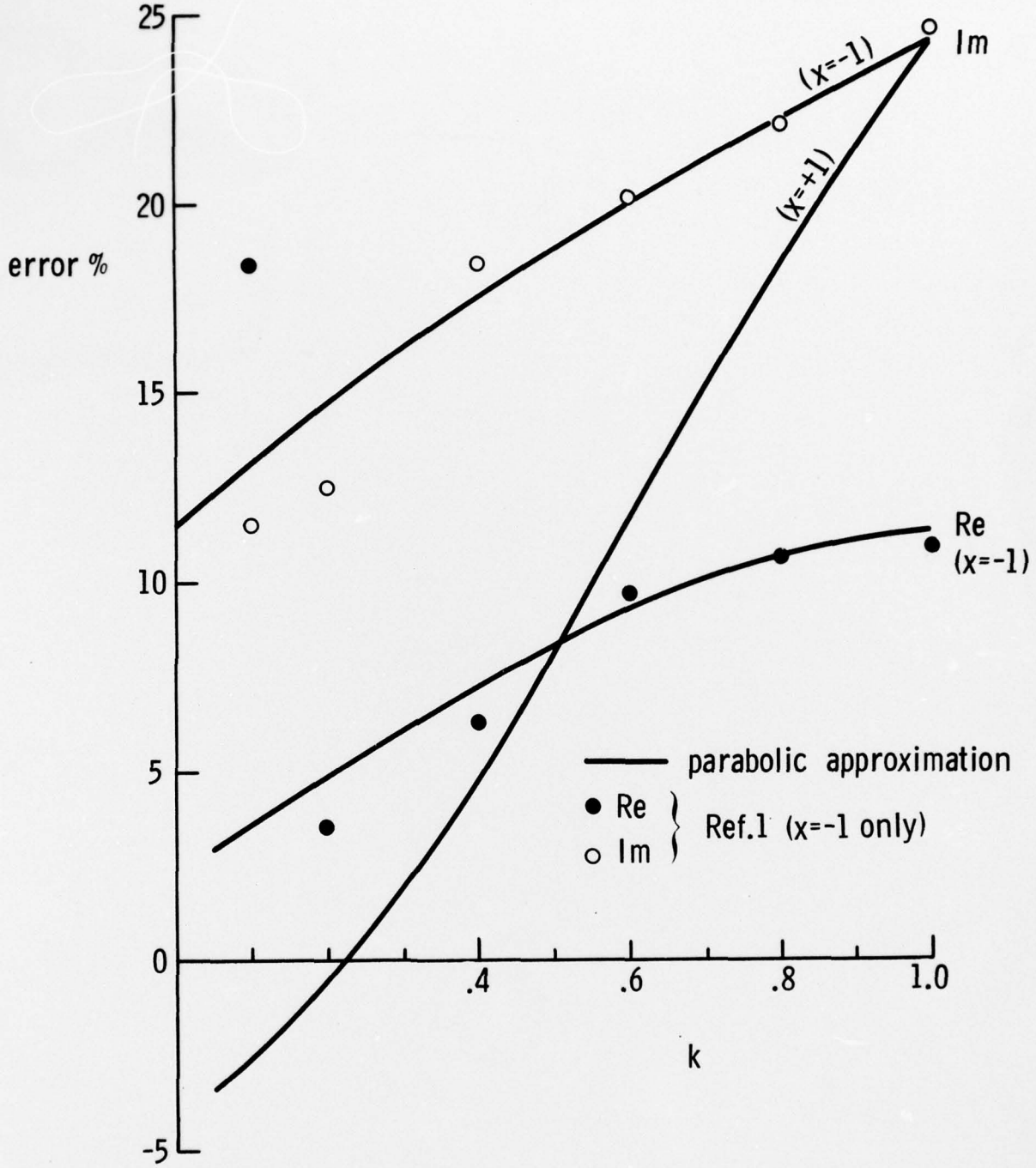

Fig. 5: Percentage errors in $w_s^{(u)}$.